Nucleon-induced preequilibrium reactions in terms of the quantum molecular dynamics

Satoshi Chiba,[1] Mark B. Chadwick,[1,2] Koji Niita,[1,3] Toshiki Maruyama,[1] Tomoyuki Maruyama,[1] and Akira Iwamoto[1]
[1]*Advanced Science Research Center, Japan Atomic Energy Research Institute, Tokai-mura, Naka-gun, Ibaraki-ken 319-11, Japan*
[2]*University of California, Theoretical Division, Los Alamos National Laboratory, Los Alamos, New Mexico 87545*
[3]*Research Organization for Information Science and Technology, Tokai-mura, Naka-gun, Ibaraki-ken 319-11, Japan*
(Received 19 October 1995)

The preequilibrium (nucleon-in, nucleon-out) angular distributions of ^{27}Al, ^{58}Ni, and ^{90}Zr have been analyzed in the energy region from 90 to 200 MeV in terms of the quantum moleculear dynamics theory. First, we show that the present approach can reproduce the measured (p,xp') and (p,xn) angular distributions leading to continuous final states without adjusting any parameters. Second, we show results of a detailed study of the preequilibrium reaction processes, the stepwise contributions to the angular distribution, comparisons with the quantum-mechanical Feshbach-Kerman-Koonin theory, and the effects of momentum distribution and surface refraction/reflection to the quasifree scattering. Finally, the present method was used to assess the importance of multiple preequilibrium particle emission as a function of projectile energy up to 1 GeV.

PACS number(s): 24.10.−i, 02.70.Ns, 25.40.Ep

I. INTRODUCTION

The nucleon-induced nuclear reactions leading to continuum states at intermediate ($E_{\rm inc} \geqslant 100$ MeV) energy range are characterized by a reaction mechanism known as the preequilibrium process [1]. In this process, particle emissions take place from simple particle-hole configurations populated as a result of a sequence of nucleon-nucleon interactions before the statistical equilibrium is attained. The angular distribution of the particles emitted from this process has generally a smooth forward peaking which is intermediate in character between the direct and compound nuclear processes. As the energy of the projectile increases, the number of particles emitted from the preequilibrium mechanism is increased and exceeds one [which is therefore called the multiple preequilibrium emission process (MPE)]. At very high energy, the reaction is often referred to as the ''spallation'' reaction, in which the average multiplicity of ejectile exceeds several or larger.

Study of the preequilibrium nuclear reactions has been an active field since the pioneering work of Goldberger [2] and Metropolis [3] based on the cascade model, and of Griffin [4] based on the exciton model. Various refinements on these approaches as well as new models both of semiclassical and quantum-mechanical followed (see, for example, Ref. [1]). The semiclassical models have been applied to analyze the energy spectra of preequilibrium particles on the outset. Later they have been improved to take account of the angular distributions of the preequilibrium process; the exciton model was improved to the generalized excition model [5–7] and the geometry dependent hybrid model [8]. The cascade model has been able to calculate the angular distributions based on the Monte Carlo technique. Furthermore, a semiclassical distorted wave theory was proposed by Luo and Kawai [9,10] who have combined the concept of quantum distorted-wave and the cascade model. They have applied this theory to calculate the one-step double-differential cross sections. Extension to the two-step process was also formulated [11]. Althouth these theories gave overall agreements with the data, there are still open questions which need further investigation for a better understanding of the preequilibrium reaction processes. For example, the backward angular distributions calculated by the semiclassical theories are often considerably smaller than the measured values. Various conjectures have been made to account for this problem [8,10,12–15]; the refraction effects at the nuclear surface, quantum diffraction, high momentum component in the momentum distribution, multistep effects, MPE, etc. So far, no simple answer seems to resolve this problem. The same problem persists even in the quantum-mechanical Feshbach-Kerman-Koonin (FKK) theory [16]; one and the only quantum-mechanical preequilibrium theory which is able to calculate the multistep direct process up to any number of steps at present. In the FKK theory, furthermore, there are some other open problems, e.g., the transition between the unbound and bound states ($P \Leftrightarrow Q$ transition) as studied recently by Watanabe *et al.* [17], and use of the normal and non-normal distorted-wave Born approximation (DWBA) matrix elements in the calculation of multistep direct components [18]. On the contrary, the cascade model has a problem at both the very forward and backward angles, where the calculated values are noticeably smaller than the experimental data. Moreover, the number of particles emitted from the preequilibrium process is limited to only 1 or 2 in many preequilibrium theories proposed so far [15,19]; an assumption which is questionable when the projectile energy becomes higher and higher.

The purpose of this paper is to study the angular distributions and MPE process in the preequilibrium (nucleon-in, nucleon-out) reaction in terms of a reaction theory based on the molecular dynamics technique, the quantum molecular dynamics (QMD) [20–22]. The QMD theory includes, in a self-consistent way, many important aspects in understanding the nucleon-induced reaction mechanisms at intermediate energy range, i.e., (1) the realistic momentum distribution of nucleons inside nuclei (including high-momentum component), (2) entrance/exit channel refraction, (3) Coulomb deflection, (4) multistep process, (5) MPE process, (6) variation of the mean-field potential due to particle-hole excitation and particle emission, (7) transition between unbound and bound

states ($P \Leftrightarrow Q$ transition in FKK theory), and (8) energy-dependent, anisotropic N-N elastic and inelastic scattering including the Pauli-bocking effect. These features make QMD a useful tool to study the nucleon-induced preequilibrium processes in a systematic manner as was first demonstrated by Peilert [22]. We are willing to show calculations of better statistics to check its ability at very backward angles for energetic ejectiles which was not clear in Ref. [22]. Furthermore, we will clarify the roles of the stepwise contributions, MPE contributions, the momentum distribution, and surface refraction/reflection to understand the basic physics of the preequilibrium reactions.

In this paper, we use the method as formulated in Ref. [23], extend the analyses given in Ref. [24], and will show that the present QMD approach gives a consistent description of the preequilibrium (p,xp') and (p,xn) angular distributions of ^{27}Al, ^{58}Ni, and ^{90}Zr targets at 90 to 200 MeV energy range in the entire angular region without any fitting procedure. Based on the excellent agreement with the data, we then proceed to study some of the open problems left in the preequilibrium processes. In Sec. II, we will give a brief explanation of the QMD to show the essential feature of our model. In Sec. III, we compare our results with experimental data and predictions of the FKK theory to find similarities and differences between these two theories. We will then give a further discussion on the angular distribution of the quasifree scattering (QFS), and the energy dependence of the MPE process.

II. BRIEF EXPLANATION OF THE QUANTUM MOLECULAR DYNAMICS

A. Equation of motion

We start from representing each nucleon (denoted by a subscript i) by a Gaussian wave packet in both the coordinate and momentum spaces in the following way:

$$f_i(\mathbf{r},\mathbf{p}) = 8\ \exp\left[-\frac{(\mathbf{r}-\mathbf{R}_i)^2}{4L}-\frac{2L(\mathbf{p}-\mathbf{P}_i)^2}{\hbar^2}\right], \tag{1}$$

where L is a parameter which represents the spatial spread of a wave packet, $\mathbf{R}_i$ and $\mathbf{P}_i$ corresponding to the centers of a wave packet in the coordinate and momentum spaces, respectively. The total one-body phase-space distribution function is taken to be simply a sum of these single-particle wave packets. The equation of motion of $\mathbf{R}_i$ and $\mathbf{P}_i$ is given, on the basis of the time-dependent variational principle, by the Newtonian equation:

$$\dot{\mathbf{R}}_i = \frac{\partial H}{\partial \mathbf{P}_i}, \quad \dot{\mathbf{P}}_i = -\frac{\partial H}{\partial \mathbf{R}_i}, \tag{2}$$

and the stochastic N-N collision term as will be described below. We have adopted the Hamiltonian H to consist of the relativistic kinetic+mass energy and the Skyrme-type effective N-N interaction [25] plus Coulomb and symmetry energy terms:

$$\begin{aligned} H = &\sum_i \sqrt{m_i^2+\mathbf{P}_i^2} \\ &+\frac{1}{2}\frac{A}{\rho_0}\sum_i \langle\rho_i\rangle + \frac{1}{1+\tau}\frac{B}{\rho_0^\tau}\sum_i \langle\rho_i\rangle^\tau \\ &+\frac{1}{2}\sum_{i,j(\neq i)} c_i c_j \frac{e^2}{|\mathbf{R}_i-\mathbf{R}_j|}\,\mathrm{erf}(|\mathbf{R}_i-\mathbf{R}_j|/\sqrt{4L}) \\ &+\frac{C_s}{2\rho_0}\sum_{i,j(\neq i)} (1-2|c_i-c_j|)\rho_{ij}, \end{aligned} \tag{3}$$

where "erf" denotes the error function, and the c_i is 1 for proton and 0 for neutron. The other symbols in Eq. (3) are defined as

$$\begin{aligned} \rho_i(\mathbf{r}) &\equiv \int \frac{d\mathbf{p}}{(2\pi\hbar)^3} f_i(\mathbf{r},\mathbf{p}) \\ &= (2\pi L)^{-3/2}\exp[-(\mathbf{r}-\mathbf{R}_i)^2/2L] \end{aligned} \tag{4}$$

and

$$\begin{aligned} \langle\rho_i\rangle &\equiv \sum_{j(\neq i)} \rho_{ij} \equiv \sum_{j(\neq i)} \int d\mathbf{r}\rho_i(\mathbf{r})\cdot\rho_j(\mathbf{r}) \\ &= \sum_{j(\neq i)} (4\pi L)^{-3/2}\exp[-(\mathbf{R}_i-\mathbf{R}_j)^2/4L]. \end{aligned} \tag{5}$$

The symmetry energy coefficient C_s is taken to be 25 MeV. The four remaining parameters, the saturation density ρ_0, Skyrme parameters A, B, and τ are chosen to be 0.168 fm^{-3}, -124 MeV, 70.5 MeV, and 4/3, respectively. These values give the binding energy/nucleon of 16 MeV at the saturation density ρ_0 and the incompressibility of 237.7 MeV [soft equation of state (EOS)] for nuclear matter limit. The only arbitrary parameter in QMD, i.e., the width parameter L, is fixed to be 2 fm^2 to give stable ground state of target nuclei in a wide mass range. These values are taken from our previous paper [23].

B. The collision term and the Pauli blocking

The stochastic nucleon-nucleon collision is taken into consideration as similar to the cascade model [23]: when the impact parameter of two nucleons is smaller than a value of $\sqrt{\sigma/\pi}$ where σ denotes the energy-dependent N-N cross section, an elastic or inelastic N-N collision takes place. We adopt a parametrization of N-N cross sections [23] which is similar to that of Cugnon [26] to take account of the in-medium effects which reduces the absolute magnitude and forward peaking of the N-N cross sections. The angular distribution of the elastic scattering was selected by the Monte-Carlo sampling method.

The Pauli blocking of the final phase space is checked after each collision. The blocking probability is calculated in the same way as the collision term in the Vlasov-Uehling-Uhlenbeck theory [27].

The parameters in the N-N cross sections were fixed in Ref. [23] and are used in this paper. Together with the parameters of the one-body dynamics given in the previous

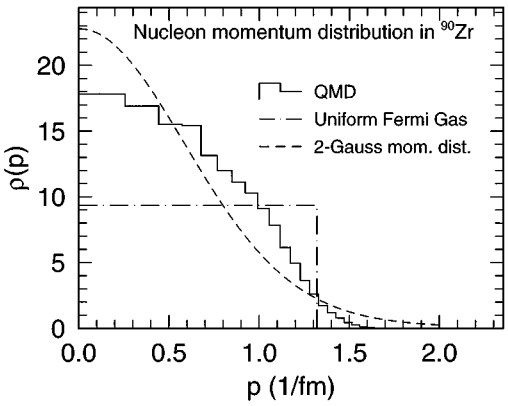

FIG. 1. Nucleon momentum distribution of ^{90}Zr. The solid histogram presents the results of QMD calculation. The smooth broken curve and the square distributions designate the two-Gaussian distribution parametrized by Haneishi and Fujita [15] and uniform Fermi gas distribution, respectively.

subsection, the equation of motion of the QMD is uniquely determined.

C. The ground state

The ground state of the target nucleus is generated by packing $\mathbf{R}_i$ and $\mathbf{P}_i$ randomly based on the Woods-Saxon type distribution in the coordinate space and corresponding local Thomas-Fermi approximation in the momentum space, seeking a configuration to reproduce the binding energy calculated by the liquid-drop model within a certain ($\pm$ 0.5 MeV) uncertainty.

The average distribution of the $\mathbf{P}_i$ obtained for ^{90}Zr is shown in Fig. 1 as the solid histogram. Experimental nucleon momentum distribution in nuclei is parametrized by a superposition of two Gaussians [14] as

$$\rho(p)=N_1(e^{(-p^2/p_0^2)}+\epsilon_0 e^{(-p^2/q_0^2)}), \tag{6}$$

where N_1 is just a normalization constant, and the parameters p_0 and q_0 are related to the Fermi momentum p_F via

$$p_0=\sqrt{2/5}p_F \quad \text{and}$$

$$q_0=\sqrt{3}p_0\,. \tag{7}$$

This distribution is plotted as a broken curve in Fig. 1, where the parameter ϵ_0 has been taken to be 0.07, about the midpoint of the range of this parameter recommended by Haneishi and Fujita. The nucleon momentum distribution in the QMD calculation has a similar shape to this two-Gaussian distribution, while the commonly adopted uniform Fermi gas distribution is just a simple square-shaped function which vanishes above the Fermi momentum. The most significant difference among these distributions is the presence of the high-momentum component in the former two distributions which is not present in the uniform Fermi gas model. The presence of the high-momentum component is a common feature of finite-nucleon systems. As a matter of fact, the momentum distribution in QMD has a very similar shape to the one obtained by the Hartree-Fock theory as compared in Fig. 6(b) of Ref. [23]. It is well known that the high-momentum component enhances the backward angular distributions [14], and as will be shown later, we obtain the same conclusion from our QMD and one-step Monte Carlo simulations. However, the effect of the difference in the momentum distribution on the angular distribution of the primary particles emitted from the quasifree scattering process was not very remarkable except at the very forward and backward angles, as will be discussed in the next section. It may worth noting here that the ground state in QMD as obtained in our work remains stable even with the high-momentum tail.

D. Decomposition into stepwise contribution in multistep reactions

For later discussion of the multistep reaction, it will be convenient to give a definition of step number in the QMD calculation which should reflect the number of collisions responsible for emission of a nucleon. First we assign a step number of 0 to each nucleon in the target nucleus. After a nucleon collides with incident nucleon, we set collision number 1 to both nucleons, inhibiting a collision between nucleons of collision number zero pair. Also, we prohibit successive collisions by the same partner. The rule of the change of the step number for each nucleon is that, if two nucleons i and j having step numbers s_i and s_j make a collision, the step numbers of both particles are modified to be s_i+s_j+1. We then identify that a nucleon is emitted from the n-step process if an isolated nucleon emitted from the nucleus has a step number of n.

As explained above, the first collision takes place only between the projectile and a nucleon in the target nucleus as expected intuitively. If one or two of these nucleons are emitted without experiencing further collisions, they contribute to the one-step process. If, on the other hand, either of these nucleons makes a further collision in the nucleus, and one or two of these nucleons involved in the second collision are emitted without further collision, they are classified as the two-step process. In the FKK theory, on the contrary, the one-step direct cross section is calculated by means of the normal DWBA method averaged over many final $1p$-$1h$ states, that is caused as a result of having one collision between the projectile and a nucleon in the target. The m-step FKK direct component is calculated by a folding integral of the $(m-1)$-step and one-step cross sections, that results after a nucleon under interest has experienced the mth collision in the system. The definitions of the step number in QMD and FKK coincide up to the step number of 3. Beyond the three-step process, however, those definitions become slightly inconsistent because QMD includes collisions between collided nucleons which are not present in FKK approach, although the probability of having such collisions in QMD is not very large.

E. Calculation of the cross section

In the calculation, many events having different impact parameter were generated. The impact parameter has been selected from a uniform distribution between 0 and a maximum value which was taken to be slightly bigger than the nuclear radius. The energy and direction of motion are stored

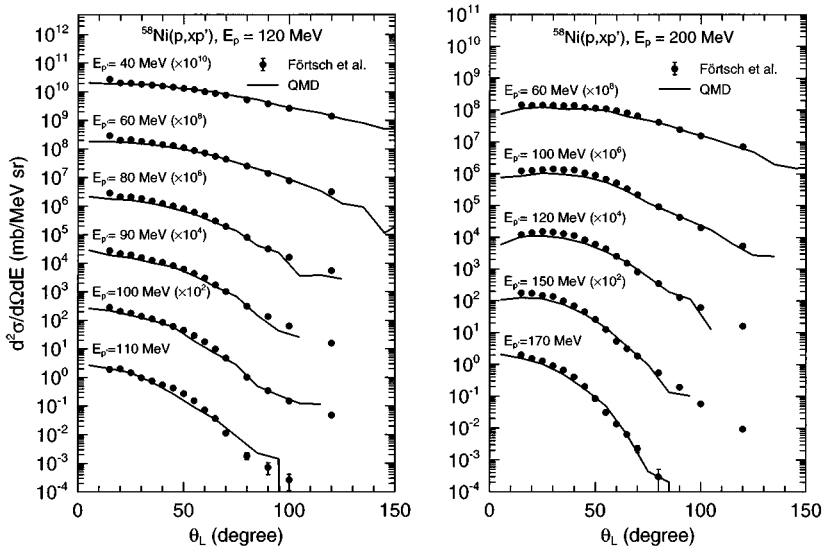

FIG. 2. The ^{58}Ni(p,xp') cross sections at E_p = 120 MeV (left) and 200 MeV (right). The data have been multiplied by the amount denoted in the parentheses.

event by event for every nucleon that becomes free (isolated from other nucleon), and finally the double-differential cross section was calculated as

$$\frac{\partial^2\sigma}{\partial E\,\partial\Omega} = \int 2\pi b\langle M(E,\Omega,b)\rangle db, \tag{8}$$

where $\langle M(E,\Omega,b)\rangle$ denotes the average multiplicity of the particle under interest (neutron or proton) emitted in the unit energy-angular interval around E and Ω for the impact paramter b event.

Typically, 50 000 events were generated to get a reasonable statistics in the stepwise double-differential cross section. In the calculation, the parameter has been fixed to the same values as in Ref. [23], without any adjustment.

III. RESULTS AND DISCUSSION

A. Comparison with experimental data

The calculated double-differential ^{58}Ni(p,xp') cross sections for incident energies at 120 and 200 MeV, and the ^{90}Zr(p,xp') and (p,xn) cross sections at 160 MeV are compared in Figs. 2 and 3 with experimental data [28–30]. The data have been shifted by the amount denoted in the parentheses. Agreement of the present calculation with the measured values is quite satisfactory from the very forward to backward angles, showing a basic ability and usefulness of our QMD approach to investigate the *N-A* reaction mechanisms in this energy regime. The problem of the underestimation at the backward angles in the semiclassical models [8,12] and the problems in the cascade model [31–33] at the very forward and backward angles are not present in the QMD approach. It must be also noticed that the QMD theory reproduces both the (p,xp') and (p,xn) cross sections simultaneously with a single set of parameters. This is a clear advantage of this approach over, e.g., the multistep direct FKK theory in which strength of the effective *N-N* cross section (the V_0 parameter) must be adjusted depending on the projectile, ejectile, target, and the incident energy [17]. In this way, it was verified that QMD gives an adjustment-free description of the preequilibrium (nucleon-in, nucleon-out) reactions at intermediate energy region in a unified manner.

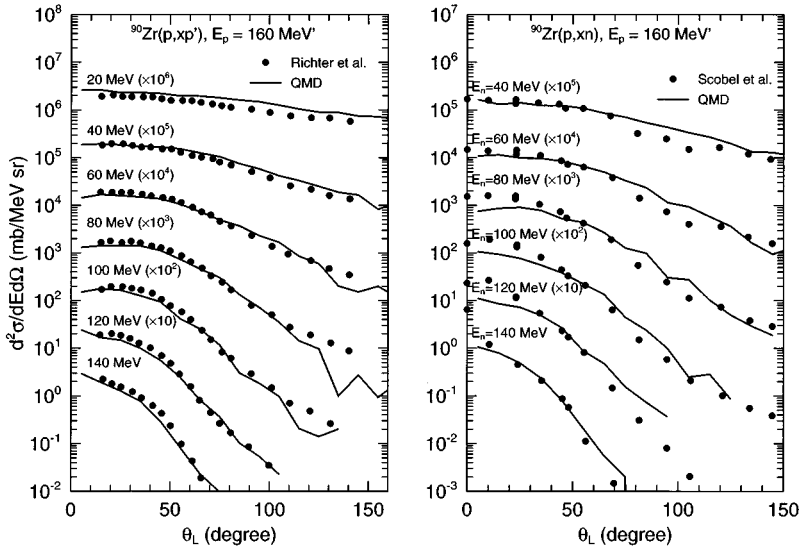

FIG. 3. The ^{90}Zr(p,xp') and (p,xn) cross sections at E_p = 160 MeV. The data have been multiplied by the amount denoted in the parentheses.

B. Stepwise contributions

In order to have a better understanding of the reason why the QMD can reproduce the measured data so well, we compare in Fig. 4 the separate contributions to ^{58}Ni(p,xp') cross sections from the one-, two-, and three-step processes and the total of all steps calculated by the QMD theory with experimental data [28]. Shown also are two arrows α and β corresponding to the angles expected from the one-step quasifree scattering process without and with the acceleration effect by the mean field, i.e.,

$$\cos\alpha = \sqrt{\frac{E_{\rm out}}{E_{\rm in}}}, \quad \cos\beta = \sqrt{\frac{E_{\rm out}-V}{E_{\rm in}-V}}, \tag{9}$$

where $E_{\rm out}$ and $E_{\rm in}$ denote the energy of the outgoing and incoming particles in the laboratory frame, respectively, while V indicates the depth of the mean-field potential which has been taken to be -50 MeV.

Figure 4 indicates the following.

The one-step process is dominant at the forward angles, while at backward angles the two and three steps are responsible to reproduce the measured cross sections.

The one-step cross section does not have a peak either at the angle α or β, instead it seems to have peaks at further forward angles for every secondary proton energy. As will be shown later, it is the Fermi motion of the target nucleon that is responsible for the shift of quasifree peak toward the forward angles.

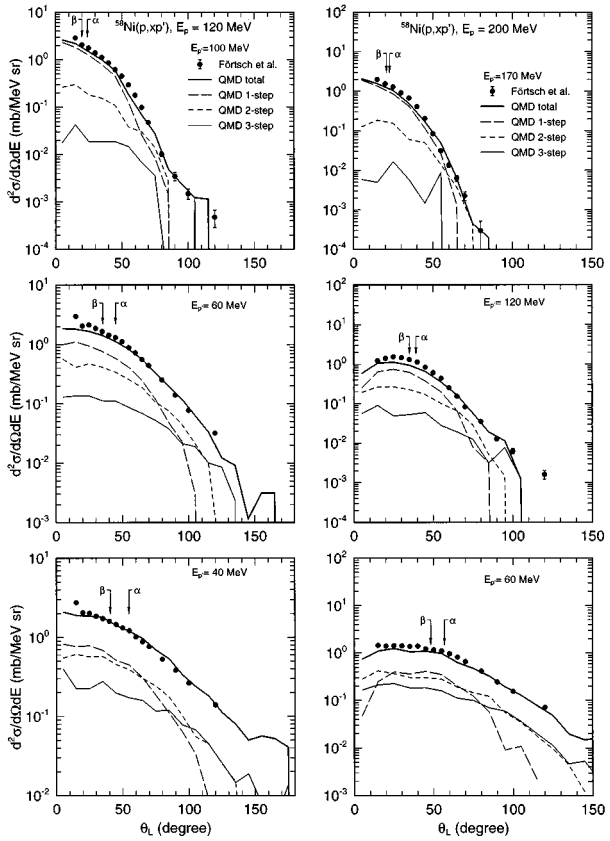

FIG. 4. The ^{58}Ni(p,xp') cross sections at $E_p = 120$ and 200 MeV. The total (thick solid line), one-step (dashed line), two-step (broken line), and three-step (thin solid line) QMD cross sections are compared with experimental data. The arrows α and β denote the position of QFS peaks as given by Eq. (9).

The one-step cross section does not fall off at the very forward angles for a high energy ejectile, i.e., at $E_{\rm out}$ close to $E_{\rm in}$. This is a special feature of QMD theory, because the one-step cross section calculated by the simple kinematical theory, as represented by the Kikuchi-Kawai formula [34], drops off sharply at the forward angles, which is the reason why the cascade model often underpredicts the cross sections at this angular region. We will show later that the refraction of the projectile and the ejectile is responsible for not having the steep drop at the forward angles.

The one-step cross section has non-negligible contribution beyond 90°. The momentum distribution, especially the high-momentum component, is the reason for this spreading out the quasifree peak toward the backward angles.

Therefore, three effects are found to be important to reproduce the measured (p,xp') cross section at the entire angular range: the refraction, the momentum distribution including the high-momentum component, and the multistep contributions. Effects of the refraction and the momentum distribution will be discussed further in later subsections.

C. Comparison with Feshbach-Kerman-Koonin model predictions

The stepwise contributions to ^{90}Zr(p,xp') and (p,xn) reactions for incident energy at 160 MeV, and ^{27}Al(p,xp') and (p,xn) reactions at 90 MeV calculated by the QMD are compared in Figs. 5, 6, 7, and 8 with those calculated by the multistep direct FKK theory and the experimental data [29,30,35,36]. It is confirmed that both theories can reproduce the measured values rather satisfactorily. The similarity between the QMD and the FKK results, as well as their abilities to reproduce the data, are rather striking considering that these two theories are based on completely different concepts; the QMD being a superposition of N-N scattering with mean-field effects, while the FKK is based on the DWBA scattering amplitudes. A noticeable difference, however, exists at the lowest ejectile energy of ^{90}Zr(p,xp') and (p,xn) reactions, where the FKK predictions are bigger than the measured data at forward angles ($\theta \geqslant 50°$), and are smaller at backward angles. The QMD results do not show such a problem. The main difference between the QMD and FKK calculations come from the difference in the one-step cross sections; the one-step FKK cross section has a prominent peak at around 30°, and drops off steeply at backward angles, while the one-step QMD cross section has much flatter shape. We will show later that the difference in the momentum distribution has little effect on the angular distribution shape from the one-step process. Therefore we conclude that the difference in the one-step QMD and FKK cross sections come from the difference in the angular distribution of the elementary process; in the QMD calculation, the one-step cross section is determined by the N-N cross section which is nearly isotropic in the c.m. of two colliding nucleons, while in the FKK theory it is determined by the DWBA. In spite of the difference in the one-step cross sections, however, the two- and three-step QMD and FKK angular distributions are very similar. This will be another confirmation of the result

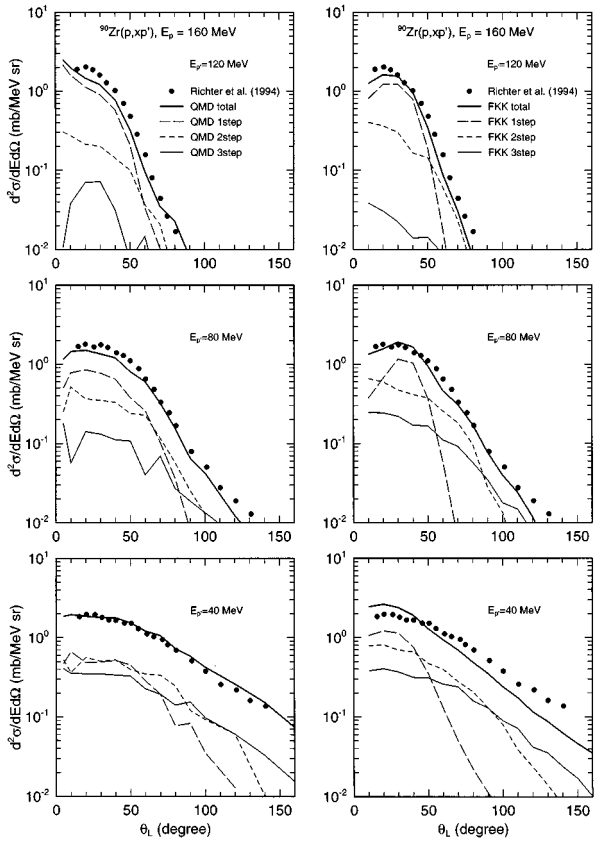

FIG. 5. The ^{90}Zr(p,xp') cross sections at $E_p=160$ MeV. The left row compares the predictions of total (thick solid line), one-step (dashed line), two-step (broken line), and three-step (thin solid line) QMD cross sections with experimental data, while the right one those of FKK theory with experimental data.

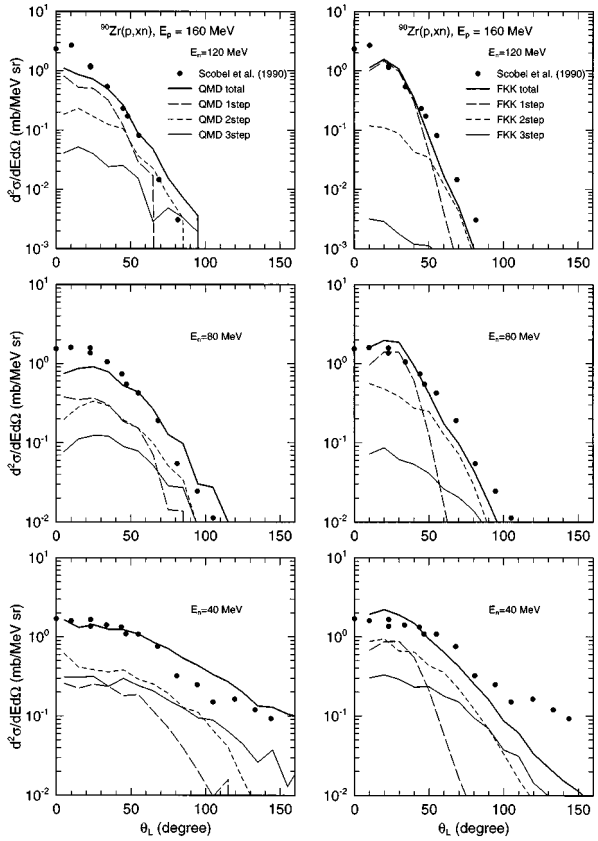

FIG. 6. The ^{90}Zr(p,xn) cross sections at $E_p=160$ MeV. The left row compares the predictions of total (thick solid line), one-step (dashed line), two-step (broken line), and three-step (thin solid line) QMD cross sections with experimental data, while the right one those of FKK theory with experimental data.

obtained by Chadwick and Obložinský [37] who have shown that the linear-momentum dependent state density obtained by the exact and statistical Gaussian solutions become identical at $2p$-$2h$ and $3p$-$3h$ states in spite of a difference in the $1p$-$1h$ state.

D. Quasifree scattering

As shown in the previous sections, the one-step quasifree scattering (QFS) cross section calculated by the QMD theory has two prominent features; it does not fall off at the very forward angles unlike the kinematical calculations [34], and it does not fall off at the backward angles as rapidly as one predicted by the FKK theory. Here, we investigate two items that may play important roles in the quasifree scattering process: the momentum distribution and the surface refraction effect.

First, we have investigated the effect of the momentum distribution to QFS angular distribution. Figure 1 indicates that the momentum distribution in the QMD calculation differs noticeably from that of the uniform Fermi gas (UFG) model, which was adopted in Kikuchi-Kawai theory. Instead of the square-shaped distribution, the momentum distribution in the QMD has a Gaussianlike shape with small portion above the Fermi momentum, which is in between the UFG and the two-Gaussian distribution suggested by Haneishi and Fujita [14].

We have compared the QMD angular distribution from the one-step (p,n) process of ^{90}Zr for incident energy at 160 MeV in the topmost parts of Fig. 9 with a simple one-step Monte Carlo calculations with momentum distributions of UFG and two Gaussian. The one-step calculation was performed as follows.

(1) Select energy of a neutron in the target either from the UFG or from the two-Gaussian distributions, assuming a nucleon binding energy of 8 MeV and Fermi energy (E_F) of 40 MeV.

(2) Make an isotropic scattering in the c.m. system of the projectile and the selected neutron in the target.

(3) The Pauli blocking effect is taken into consideration with a blocking probability given by

$$P_{\text{block}}=1-[1-\theta(E_{\text{F}}-E_1')][1-\theta(E_{\text{F}}-E_2')], \quad (10)$$

where E_1' and E_2' denote the energies of scattered particles.

(4) If the collision is not blocked, the energy and angle of the scattered particle (which originally was in the target) in the laboratory frame is recorded.

(5) Repeat items (1) to (4) many times.

(6) The absolute magnitudes of these one-step cross sections were normalized to the corresponding one-step QMD cross section.

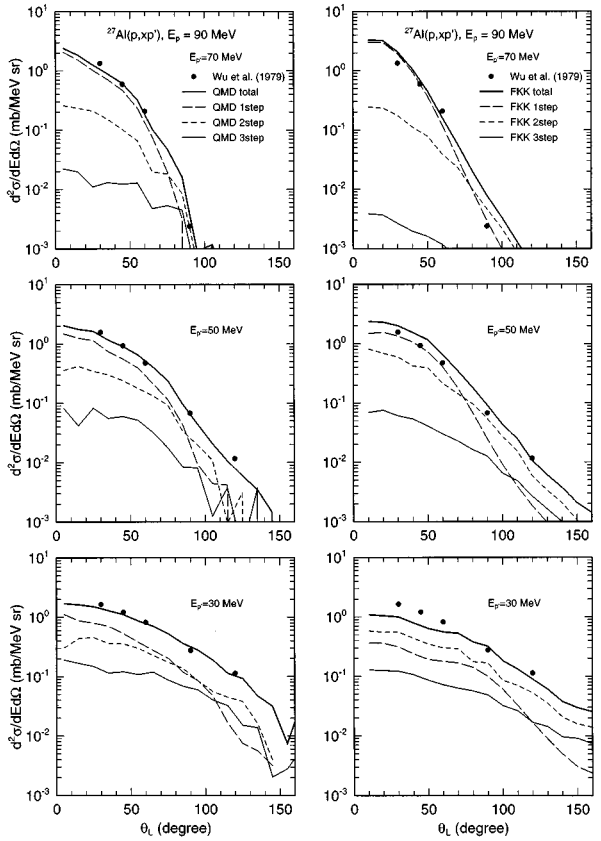

FIG. 7. The $^{27}\mathrm{Al}(p,xp')$ cross sections at $E_p=90$ MeV. The left row compares the predictions of total (thick solid line), one-step (dashed line), two-step (broken line), and three-step (thin solid line) QMD cross sections with experimental data, while the right one those of FKK theory with experimental data.

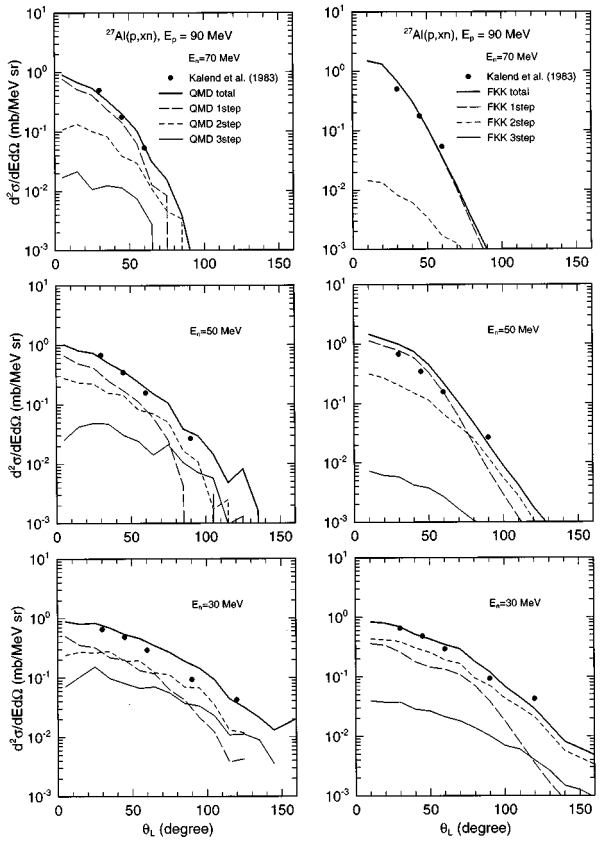

FIG. 8. The $^{27}\mathrm{Al}(p,xn)$ cross sections at $E_p=90$ MeV. The left row compares the predictions of total (thick solid line), one-step (dashed line), two-step (broken line), and three-step (thin solid line) QMD cross sections with experimental data, while the right one those of FKK theory with experimental data.

The upper two figures in Fig. 9 show that, in the main part of the angular distribution, the difference between the UFG and the two-Gaussian results is not very noticeable. The main difference lies at the very forward and backward angles, where the UFG result exhibits a steep drop, while the two-Gaussian result shows a slower decrease. This is definitely due to the high-momentum component in the two-Gaussian momentum distribution, because this difference disappears when we cut the high-momentum component in the two-Gaussian distribution. Also, it is clear that the two distributions do not give the QFS peak at angles denoted by α or β, but give a peak at more forward angles. Therefore, the Fermi motion of target nucleons was found to shift the QFS peak to the forward angles. The peaks are, however, not very prominent in both cases; the Fermi motion tends to wash out the QFS peak. The one-step QMD cross section is in very good accord with both one-step results at intermediate angles. As a matter of fact, the angle beyond which the QMD cross section vanishes lies in between the corresponding angles of the UFG and two-Gaussian results, because the momentum distribution in QMD lies in between these two distributions as shown in Fig. 1. However, the QMD results do not show decreasing angular shapes toward 0°. Therefore, the reason why the one-step QMD results have large cross sections in the vicinity of 0° was not explained by the Fermi motion of the target nucleons.

In the lower parts of Fig. 9, we have compared two kinds of one-step QMD cross sections, one with the full calculation, and one which cuts the refraction effects. The one-step QMD results without the refraction show a shape very similar to the one calculated with the uniform Fermi gas model, with a steep drop at the very forward angles, while the refraction effect totally washes out this steep decrease. Thus it became clear now that it is the refraction effect by the mean field which causes a nondecreasing one-step cross section in the QMD calculation at 0° region. This effect, together with contributions from the two-, three-, and higher steps, makes the total QMD cross sections to have a smoothly varying angular shape from the very forward to backward angles, which is in good accord with the measured data. Therefore, we conclude that the Fermi motion of target nucleons, mean field refraction, and the multistep effects are essential in predicting the angular distributions of preequilibrium (N,N') cross section in this energy range.

In the present calculation, the mean-field refraction effect washes out the decrease of the cross section at the very forward angle. This result, at first glance, may look completely opposite to the one obtained with the geometry-dependent hybrid model (GDH) where the steep increase at the forward angle is washed out by the surface refraction at low incident energy (e.g., Fig. 4 of Ref. [8]). At higher incident energy, however, the GDH predicts decreasing angular shape toward

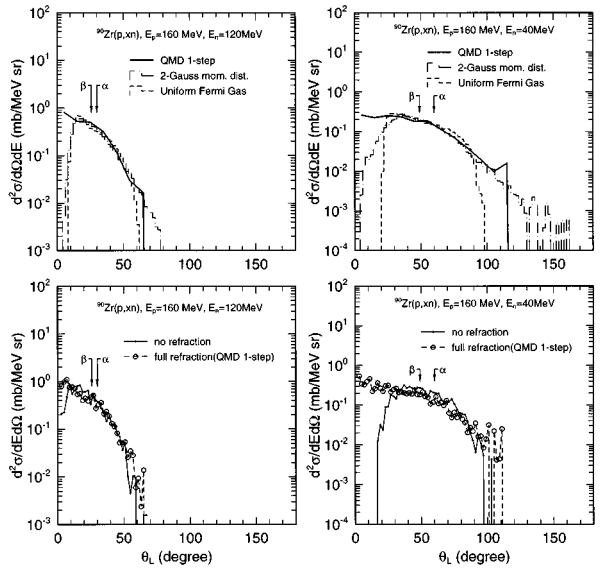

FIG. 9. The ^{90}Zr(p,xn) cross sections at $E_p = 160$ MeV and $E_n = 120$ (left figures) and $E_n = 40$ (right) MeV. The upper two figures compare one-step QMD cross section (solid lines) with simple one-step Monte Carlo calculations assuming the uniform Fermi gas (broken histograms) and two-Gaussian (long-broken histograms) momentum distributions of target nucleons. The lower two figures compare the full one-step QMD cross section with a calculation ignoring the refraction effects.

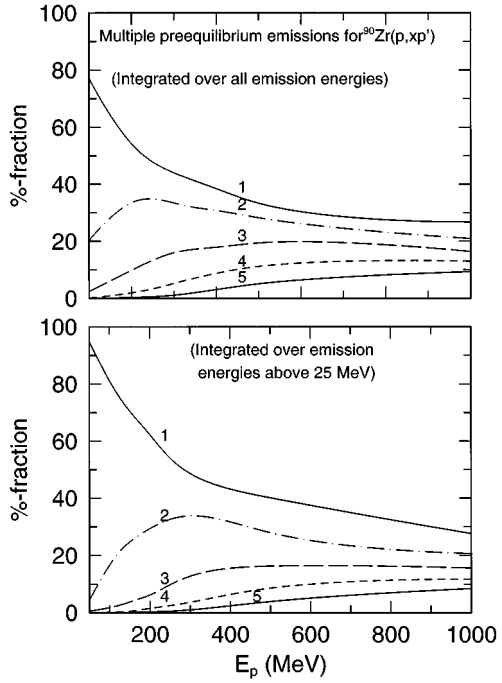

FIG. 10. Relative contributions of multiparticle emissions as a function of the incident energy calculated by the QMD. The upper figure includes all emission energies, whereas the lower figure considers only emission energies above 25 MeV (the preequilibrium regime).

0° that is smeared out when the refraction effect is considered (20 MeV *n* of Fig. 6 in Ref. [8]), which is in good agreement with the present result. The reason why the GDH calculation has such a steep increase at the forward angle of low-incident energy is unclear to us: at least as far as the one-step process is concerned, the cross section must have a decrease as a result of kinematical restriction and Pauli-principle as Kikuchi-Kawai formula indicates. It may be just a result of finite angle binning carried out by Blann *et al.* In the QMD calculation, both the Fermi motion and the surface refraction effect are taken into account by means of the equation of motion [i.e., Eq. (2)] in a unified manner, and any arbitrariness is not involved as is the case of GDH to introduce the surface refraction.

It must be noticed that the refraction effect in our calculation might be overemphasized due to the fact that momentum dependence is not included in the effective *N-N* force that changes the mean-field potential from attractive at low energy to repulsive at energies higher than approximately 200 to 300 MeV region. However, the relativistic approach on the optical potential gives a wine-bottle-bottom shaped potential that remains attractive at the surface regime even at high energy region where the potential at the nuclear interior becomes significantly repulsive [38,39]. Moreover, according to Gadioli and Hodgson [1], inclusion of the momentum-dependent potential leads to two opposite consequences. (a) It reduces the importance of refractions of nucleons by reducing the potential at the 200–300 MeV region. This effect increases the probability of emission of particles. However, (b) the particles in the mean-field will have on the average lower kinetic energies, and (due to the increase of the *N-N* cross section) smaller mean free paths with the consequence that the nuclear transparency is decreased. These two effects tend to cancel each other, and the net effect of the momentum-dependent potential might be substantially reduced.

E. Multiple preequilibrium emission

In Ref. [24], we have shown that the QMD gives results consistent with the FKK theory for the energy spectra of first and second particles emitted from the preequilibrium process up to projectile energy of 200 MeV. Recently, there is a growing interest in nucleon-induced reactions up to 1 GeV region stimulated by the results obtained at LAMPF facility on the Pb(n,x) and Fe(p,x) reactions [40,41] and from a practical point of view [42,43]. Our QMD approach can be applied to above 1 GeV without any change, and there is no limitation in the number of particles emitted from the preequilibrium process. Therefore we have extended the analysis given in Ref. [24] up to 1 GeV, and investigated the importance of MPE process as a function of projectile energy.

We have shown in Fig. 10 the QMD results for the fractional contributions to the total number of inclusive proton emission contributed by the particles emitted as the first, second, third, fourth, and fifth particles. The upper figure shows the percentage when all emission energies are considered, while the lower figure includes only emissions of above 25 MeV (as defined in the preequilibrium regime in Ref. [24]). The lower figure shows that the sum of the contribution by the third, fourth, and fifth particles in the preequilibrium process occupies a fraction of about 30% at the incident energy of 500 MeV, and almost 50% at 1 GeV, showing a clear

necessity of including the MPE process more than two particles.

IV. SUMMARY

We have shown that the quantum molecular dynamics (QMD) model can reproduce the measured data for intermediate-energy nucleon-induced preequilibrium nucleon-emission process without any adjustment of the underlying parameters. Based on this success, we then have studied some of the open problems in the preequilbrium reactions: the angular distribution and the multiple preequilibrium particle emission (MPE). The QMD calculation has not shown the prominent quasifree scattering peak, which is consistent with the measured data. The reason of the overall agreement with the data was explained by the Fermi motion of target nucleons, the refraction of projectile and ejectile, and contribution from the multistep processes. The MPE process beyond two-particle emission was found to exceed 30% at 500 MeV and reaches almost 50% at 1 GeV, thus becoming the major reaction mechanism at this energy region.

ACKNOWLEDGMENTS

The authors would like to thank Professor M. Kawai and Dr. Y. Watanabe of Kyushu University and Professor H. Horiuchi and the late E. I. Tanaka of Kyoto University for valuable comments and discussions. This work was performed in part under the auspices of the U.S. Department of Energy by the Los Alamos National Laboratory under Contract No. W-7405-EWG-360.

[1] For example, E. Gadioli and P.E. Hodgson, *Pre-Equilibrium Nuclear Reactions* (Clarendon Press, Oxford, 1992).
[2] M.L. Goldberber, Phys. Rev. **74**, 1269 (1948).
[3] N. Metropolis, R. Bivins, M. Storm, J.M. Miller, G. Friedlander, and A. Turkievich, Phys. Rev. **110**, 204 (1958).
[4] J.J. Griffin, Phys. Rev. Lett. **17**, 478 (1966).
[5] G. Mantzouranis, H.A. Weidenmüller, and D. Agassi, Phys. Lett. **57B**, 220 (1975).
[6] J.M. Akkermans, H. Gruppelaar, and G. Reffo, Phys. Rev. C **22**, 73 (1980).
[7] A. Iwamoto and K. Harada, Nucl. Phys. **A419**, 274 (1984).
[8] M. Blann, W. Scobel, and E. Plechaty, Phys. Rev. C **30**, 1493 (1984).
[9] Y.L. Luo and M. Kawai, Phys. Rev. C **43**, 2367 (1991).
[10] Y. Watanabe and M. Kawai, Nucl. Phys. **A560**, 43 (1993).
[11] M. Kawai and H.A. Weidenmüller, Phys. Rev. C **45**, 1856 (1992).
[12] C. Costa, H. Gruppelaar, and J.M. Akkermans, Phys. Rev. C **28**, 587 (1983).
[13] M.B. Chadwick and P. Obložinský, Phys. Rev. C **44**, R1740 (1991).
[14] Y. Haneishi and T. Fujita, Phys. Rev. C **33**, 260 (1986).
[15] M.B. Chadwick, P.G. Young, D.C. George, and Y. Watanabe, Phys. Rev. C **50**, 996 (1994).
[16] H. Feshbach, A. Kerman, and S. Koonin, Ann. Phys. (N.Y.) **125**, 429 (1980).
[17] Y. Watanabe, A. Aoto, H. Kashimoto, S. Chiba, T. Fukahori, K. Hasegawa, M. Mizumoto, S. Meigo, M. Sugimoto, Y. Yamanouti, N. Koori, M.B. Chadwick, and P.E. Hodgson, Phys. Rev. C **51**, 1891 (1995).
[18] T. Udagawa, K.S. Low, and T. Tamura, Phys. Rev. C **28**, 1033 (1983).
[19] M. Blann and H.K. Vonach, Phys. Rev. C **28**, 1475 (1983).
[20] J. Aichelin, G. Peilert, A. Bohnet, A. Rosenhauser, H. Stöcker, and W. Greiner, Phys. Rev. C **37**, 2451 (1988).
[21] T. Maruyama, A. Ohnishi, and H. Horiuchi, Phys. Rev. C **45**, 2355 (1992).
[22] G. Peilert, J. Konopka, H. Stöcker, W. Greiner, M. Blann, and M.G. Mustafa, Phys. Rev. C **46**, 1457 (1992).
[23] K. Niita, S. Chiba, T. Maruyama, T. Maruyama, H. Takada, T. Fukahori, Y. Nakahara, and A. Iwamoto, Phys. Rev. C **52**, 2620 (1995).
[24] M.B. Chadwick, S. Chiba, K. Niita, T. Maruyama, and A. Iwamoto, Phys. Rev. C **52**, 2800 (1995).
[25] T.H.R. Skyrme, Nucl. Phys. **9**, 615 (1959).
[26] J. Cougnon, T. Mizutani, and J. Vandermeule, Nucl. Phys. **A352**, 505 (1981).
[27] G.F. Bertch and S. Das Gupta, Phys. Rep. **160**, 189 (1988).
[28] S.V. Förtsch, A.A. Cowley, J.J. Lawrie, D.M. Whittal, J.V. Pilcher, and F.D. Smit, Phys. Rev. C **43**, 691 (1991).
[29] W.A. Richter, A.A. Cowley, G.C. Hillhouse, J.A. Stander, J.W. Koen, S.W. Steyn, R. Lindsay, R.E. Julies, J.J. Lawrie, J.V. Pilcher, and P.E. Hodgson, Phys. Rev. C **49**, 1001 (1994).
[30] W. Scobel, M. Tranbandt, M. Blann, B.A. Pohl, B.R. Remington, R.C. Byrd, C.C. Foster, R. Bonetti, C. Chiesa, and S.M. Grimes, Phys. Rev. C **41**, 2010 (1990).
[31] N. Yoshizawa, K. Ishibashi, and H. Takada, J. Nucl. Sci. Technol. **32**, 601 (1995).
[32] H. Takada, J. Nucl. Sci. Technol. (submitted).
[33] H.W. Bertini, G.D. Harp, and F.E. Bertland, Phys. Rev. C **10**, 2472 (1974).
[34] K. Kikuchi and M. Kawai, *Nuclear Matter and Nuclear Reactions* (North-Holland, Amsterdam, 1968).
[35] J.R. Wu, C.C. Chang, and H.D. Holmgren, Phys. Rev. C **19**, 698 (1979).
[36] A.M. Kalend, B.D. Anderson, A.R. Baldwin, R. Madey, J.W. Watson, C.C. Chang, H.D. Holmgren, R.W. Koontz, J.R. Wu, and H. Machner, Phys. Rev. C **28**, 105 (1983).
[37] M.B. Chadwick and P. Obložinský, Phys. Rev. C **46**, 2028 (1992).
[38] L. Rikus and H.V. Von Geramb, Nucl. Phys. **A426**, 496 (1984).
[39] S. Hama, B.C. Clark, E.D. Cooper, H.S. Sherif, and R.L. Mercer, Phys. Rev. C **41**, 2737 (1990).
[40] H. Vonach, A. Pavlik, M.B. Chadwick, R.C. Haight, R.O. Nelson, S.A. Wender, and P.G. Young, Phys. Rev. C **50**, 1952 (1994).
[41] H. Vonach (private communication).
[42] For example, Proceedings of a Specialists' Meeting on Intermediate Eenrgy Nuclear Data: Models and Codes, OECD, 1994 (unpublished).
[43] Rolf Michel and Pierre Nagel, ''Specifications for an International Codes and Model Intercomparison for Intermediate Energy Activation Yields,'' Report No. NEA/NSC/DOC(95)8, OECD/NEA (1995).